Asialoglycoprotein Receptor and Hepatic Blood Flow Using Technetium-99m-DTPA-Galactosyl Human Serum Albumin

Kenji Miki, Keiichi Kubota, Norihiro Kokudo, Yusuke Inoue, Yasutsugu Bandai and Masatoshi Makuuchi
Second Department of Surgery and Department of Radiology, Faculty of Medicine, University of Tokyo; Department of Surgery, Cancer Institute Hospital; and Department of Surgery, Central Hospital of Social Health Insurance, Tokyo, Japan

Asialoglycoprotein receptor (ASGP-R) amount and hepatic blood flow were quantitatively measured by using a newly developed kinetic model of ^{99m}Tc-labeled diethylenetriaminepentaacetic acid-galactosyl human serum albumin (^{99m}Tc-GSA) in which receptor-mediated endocytosis and receptor recycling were considered. **Methods:** Five healthy volunteers were intravenously injected 3-mg and 9-mg ^{99m}Tc-GSA doses. The absolute amounts of ^{99m}Tc-GSA in the liver and extrahepatic blood were estimated from the time-activity curves for the liver, heart and lung. The metabolic process was represented by five differential equations with 10 parameters as variables. To estimate total receptor amount (R_{total}), hepatic plasma flow (Q) and hepatic plasma volume (V_h), other parameters were fixed and estimated by analyzing their data with the least-squares method. Nineteen patients with liver diseases were given a 3-mg dose, and the data were analyzed to estimate R_{total}, Q and V_h. **Results:** The values of the fixed parameters were estimated as follows: dissociation constant, 0.032 μM; rate constant for internalization, 0.604 min^{-1}; and ratio of surface receptors to total receptors, 6.1%. The fitted liver uptake curve corresponded well to the measured data. The simulated liver uptake curve was significantly influenced by R_{total} and Q in cases with normal receptor amounts. Analysis in patients with normal livers, chronic hepatitis and liver cirrhosis showed statistically significant differences in their R_{total} values, but not in their Q or V_h values. The s.e. values of R_{total}, Q and V_h for normal livers were small, and the s.e. values of Q and V_h were high for cirrhotic livers. **Conclusion:** This method is useful for measuring ASGP-R amount and hepatic blood flow simultaneously based on dynamic images, without the need for blood sampling, and reflects the cellular transport of asialoglycoproteins and the ASGP-R recycling mechanism.

Key Words: technetium-99m-GSA; pharmacokinetics; asialoglycoprotein receptor; receptor-mediated endocytosis; receptor recycling

J Nucl Med 1997; 38:1798–1807

Asialoglycoprotein (ASGP) was discovered by Morell et al. (*1*) and Pricer et al. (*2*) and is a general term for desialylated glycoprotein, which is specifically taken into mammalian hepatocytes by binding to ASGP receptors (ASGP-Rs). The ASGP metabolic process has been studied extensively by several investigators (*3–10*). ASGP is recognized on the surface of hepatocytes and is bound by ASGP-R in a second-order chemical reaction (*3–5*). The ASGP–ASGP-R complex on the cell surface is subsequently specifically taken into cytoplasm by endocytotic internalization and transferred to lysosomes (*5–9*). ASGP-R is then dissociated from ASGP and recycled to the cell surface. ASGP is catabolized in the lysosomes and excreted into the bile (*10*).

The number of ASGP-Rs decreases in patients with chronic liver diseases. Their ASGP metabolism is impaired (*11*), and their serum ASGP levels increase as a result. Technetium-99m-labeled diethylenetriaminepentaacetic acid-galactosyl human serum albumin (^{99m}Tc-GSA) is a neoglycoalbumin developed for hepatic imaging (*12*), and its metabolism is influenced by ASGP-R binding activity. Several parameters obtained by analyzing the dynamic images of ^{99m}Tc-GSA have been shown to correlate well with other liver functional indicators, such as prothrombin time and indocyanine green retention rate (*13,14*).

Although compartment models for evaluating hepatic blood flow and receptor binding activity by using labeled neoglycoalbumin were developed by Vera et al. (*15,16*) and Ha-Kawa et al. (*17*), they did not take receptor-mediated endocytosis or receptor recycling into consideration, whereas our method, using a new compartment model, is unique in referring to these mechanisms. The details of the new compartment model are described and its adequacy is discussed in this article.

MATERIALS AND METHODS

Human Subjects

The subjects of this study consisted of 5 healthy volunteers and 19 patients with liver diseases. The former group received 3 mg (0.040 μmol) and 9 mg (0.118 μmol) of ^{99m}Tc-GSA, and their data were analyzed to estimate unknown parameters and develop a new program for evaluating liver function. The latter group was given 3 mg of ^{99m}Tc-GSA, and their data were analyzed by using the newly developed program. The liver disease group consisted of five patients with metastatic liver tumors in otherwise normal livers (N group), six with chronic hepatitis (CH group) and eight with liver cirrhosis (LC group). The protocol was approved by the Human Subject Review Committee of Central Hospital of Social Health Insurance. Informed consent was obtained from each subject before the ^{99m}Tc-GSA study.

Data Acquisition

Technetium-99m-GSA was supplied as the labeled agent. The radioactivity of ^{99m}Tc-GSA was 3 mg/185 MBq at the time of calibration. A 3-mg dose of ^{99m}Tc-GSA was injected into each subject through a cubital vein, and in the healthy volunteers, the test was repeated with a 9-mg dose of ^{99m}Tc-GSA after an interval of more than 1 wk after the first examination. The radioactivity of the 9 mg of ^{99m}Tc-GSA was adjusted to be less than 300 MBq by time decay.

Dynamic images were obtained with the subject in the supine position under a large field-of-view gamma camera with a low-energy, all-purpose, parallel-hole collimator. Computer acquisition of gamma camera data was started immediately after injection and was stopped after 60 min in the 5 healthy volunteers and after 30 min in the 19 patients. Digital images (64 × 64 pixels) were acquired at 2-sec frames for the first 2 min after injection and at

Received Sep. 4, 1996; revision accepted Jan. 13, 1997.
For correspondence or reprints contact: Kenji Miki, MD, Second Department of Surgery, Faculty of Medicine, University of Tokyo, 7-3-1 Hongo, Bunkyo-Ku, Tokyo 113, Japan.

TABLE 1
Symbols Used in This Study

Symbols	Description	Units	Equations*
$L(t)$	Count rate in the liver ROI	kct/sec	1
$H(t)$	Count rate in the heart ROI	kct/sec	1, 3
$Lu(t)$	Count rate in the lung ROI	kct/sec	3
$BS(t)$	Radioactivity of blood samples	counts/min	
$B(t)$	Corrected count rate in the heart	kct/sec	**3**, 4, 7
Δt	Acquisition time of the individual frame	sec	2
$L_{correct}(t)$	Corrected count rate in the liver	kct/sec	**1**, 4, 6, 29
$\sigma^2(t)$	Variance of $L_{correct}(t)$	kct^2/sec^2	**2**, 29
L_{total}	Count rate of the total injected dose accumulated in the liver	kct/sec	**6**, **7**, 26, 31
ΔL_{total}	Estimated error of L_{total}	kct/sec	
k_B	Detector sensitivity coefficient of $B(t)$	$\mu mol \cdot sec/kct$	**4**, 5, 7
k_L	Detector sensitivity coeffficient of $L_{correct}(t)$	$\mu mol \cdot sec/kct$	**4**, 5, 6
$LD(t)$	Amount of ^{99m}Tc-GSA in the liver	μmol	4, **6**, 8
$BD(t)$	Amount of ^{99m}Tc-GSA in extrahepatic plasma	μmol	4, **7**, 8
$f_d(t)$	Ratio of V_e to the actual distribution volume	No units	**8**, 9, 33
D_1	^{99m}Tc-GSA in the extrahepatic plasma	μmol	9, **14**
D_2	^{99m}Tc-GSA in hepatic plasma	μmol	9, 10, **22**, 23, 26
D_3	^{99m}Tc-GSA binding to receptor on the cell surface	μmol	10, 11, 13, 22, **23**, 26
D_4	^{99m}Tc-GSA binding to receptor in the cytoplasm	μmol	11, 12, 13, **16**, 26
D_5	^{99m}Tc-GSA metabolized in the cytoplasm	μmol	**17**, 26
R_s	Unbound receptor on the cell surface	μmol	10, 13, **20**
R_i	Unbound receptor in the cytoplasm	μmol	13
R_{total}	Total receptor amount	μmol	13, 22, 23
TPV	Total plasma volume	liters	**27**, **28**, 31
V_e	Extrahepatic plasma volume	liters	9
V_h	Hepatic plasma volume	liters	9, 10, 19, 22, 23, **31**
$T_{1\text{-}2}$	Net transport of ^{99m}Tc-GSA from C1 to C2	$\mu mol/min$	**9**, 14, 15, 22, 23
$T_{3\text{-}4}$	Net transport of ligand–receptor complex from C3 to C4	$\mu mol/min$	**11**, 15, 16, 22, 23
$T_{4\text{-}5}$	Transport of ^{99m}Tc-GSA from C4 to C5	$\mu mol/min$	**12**, 16, 17, 22, 23
Q	Hepatic plasma flow	liters/min	9
K_d	Dissociation constant on the cell surface	μM	**10**, 22, 23
k_{in}	Rate constant for endocytosis	min^{-1}	11
k_{out}	Rate constant for exocytosis	min^{-1}	11
k_r	Rate constant for dissociation in the cytoplasm	min^{-1}	12
k_e	Rate constant for excretion into the bile	min^{-1}	17
$r_{s\text{-}i}$	Ratio of receptor on the cell surface to receptor pool	No units	**13**, 22, 23
$f(t)$	Simulated count rate in the liver ROI	kct/sec	**26**, 29
SS_w	Weighted sum of squares		29
$s.e._p$	s.e. of each parameter		32
Δp	Error caused by ΔL_{total}		32

*Numbers in bold indicate main equations using these symbols.

30-sec frames from 2 to 60 min or 30 min after injection. Heparinized blood samples were taken from a contralateral cubital vein of the healthy volunteers at 3, 5, 10, 15, 30 and 60 min after injection. The radioactivity of the blood samples [BS(t)] was measured in a well scintillation counter.

Regions of interest (ROIs) were drawn over the whole liver in the images 29.5–30 min after injection and over the heart and right lung areas in the images 2.0–2.5 min after injection at the same distance from the liver ROI. The respective ROIs for the heart and lung were adjusted to almost the same size. Then, time–activity curves for the liver [L(t), in kilocounts (kct)/sec], heart [H(t), in kct/sec] and lung [Lu(t), in kct/sec] were generated using these ROIs, which were corrected according to radioactive decay. All symbols used in this study are listed in Table 1.

Determination of Liver Uptake Starting Time and Correction of Liver Time–Activity Curve

The time when the descending aorta was initially visualized was taken to be the starting time of liver uptake (t_0, in min). Counts in the liver ROI before t_0 were attributed to radioactivity in the heart and lung. True liver uptake [$L_{correct}(t)$, in kct/sec] was calculated by subtracting H(t) from L(t), according to the ratio of the total counts of L(t) and H(t) before t_0:

$$L_{correct}(t) = L(t) - \frac{\int_0^{t_0} L(t)dt}{\int_0^{t_0} H(t)dt} \times H(t). \quad \text{Eq. 1}$$

Based on a Poisson distribution for nuclear decay, the variance of $L_{correct}(t)$ at each measured point was calculated thus:

$$\sigma^2 = \frac{L(t)}{\Delta t} + \left(\frac{\int_0^{t_0} L(t)\,dt}{\int_0^{t_0} H(t)\,dt} \right)^2 \times \frac{H(t)}{\Delta t}, \quad \text{Eq. 2}$$

where Δt is the acquisition time of the individual frame.

Correction of Heart Time–Activity Curve

The heart time–activity data were corrected by subtracting Lu(t) from H(t), after correcting for pixel number:

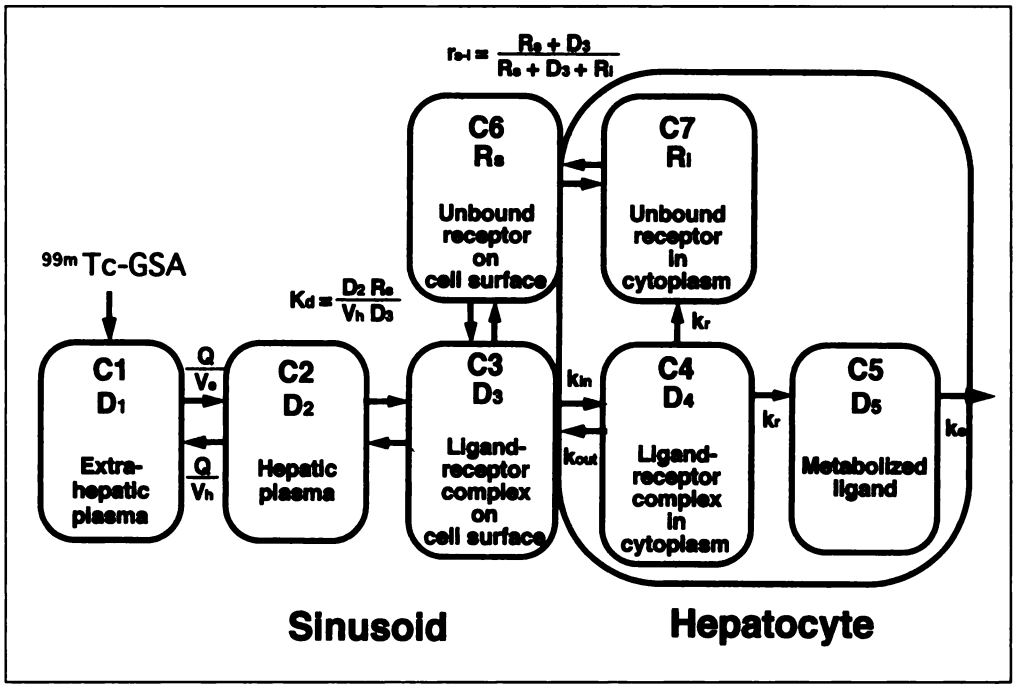

FIGURE 1. Compartment model of ^{99m}Tc-GSA. The metabolic process of ^{99m}Tc-GSA (C1 → C2 → C3 → C4 → C5) and receptor recycling (C4 → C7 → C6 → C3 → C4) are represented. In this model, K_d, k_{in}, k_{out}, k_r and $r_{s\text{-}i}$ were assumed to be unchangeable, and Q, V_h and $R_{total} = R_s + R_i + D3 + D4$ were estimated for each subject.

$$B(t) = H(t) - \frac{\text{number of pixels in the heart ROI}}{\text{number of pixels in the lung ROI}} \times Lu(t), \quad \text{Eq. 3}$$

where B(t) (kct/sec) is the corrected heart time–activity data, representing the radioactivity in extrahepatic blood.

The H(t), Lu(t), B(t) and BS(t) values, divided by the values obtained 3 min after injection, were expressed as H(t)/H(3), Lu(t)/H(3), B(t)/B(3) and BS(t)/BS(3), respectively, and compared to each other. The mean absolute errors of B(t)/B(3) and H(t)/H(3) were calculated as the mean absolute differences between B(t)/B(3) and BS(t)/BS(3) and between H(t)/H(3) and BS(t)/BS(3), respectively, at all points measured.

Estimation of the Amount of Technetium-99m-GSA in the Liver and Extrahepatic Plasma

Assuming that the distribution of the interstitial space and urinary excretion are negligible, the following equation was derived:

$$\text{injected dose } (\mu\text{mol}) = LD(t) + BD(t) = k_L \times L_{correct}(t) + k_B \times B(t). \quad \text{Eq. 4}$$

Therefore, $L_{correct}(t)$ is expressed as a linear function of B(t):

$$L_{correct}(t) = -\frac{k_B}{k_L} \times B(t) + \frac{\text{injected dose}}{k_L}. \quad \text{Eq. 5}$$

The y-intercept (L_{total} = injected dose/k_L, in kct/sec), estimated error of the y-intercept (ΔL_{total}, in kct/sec) and regression slope (slope = $-k_B/k_L$) were estimated from the data during the 2–30 min after injection by linear regression with errors in both coordinates (*18*). From Equations 4 and 5, LD(t) and BD(t) were calculated as the following equations:

$$LD(t) = k_L \times L_{correct}(t) = \frac{\text{injected dose}}{L_{total}} \times L_{correct}(t) \quad \text{Eq. 6}$$

and

$$BD(t) = k_B \times B(t) = \frac{\text{slope} \times \text{injected dose}}{L_{total}} \times B(t). \quad \text{Eq. 7}$$

Plasma Concentration in the Early Phase after Injection

Because ^{99m}Tc-GSA is assumed to be distributed nonuniformly in extrahepatic blood and the actual distribution volume is smaller than the extrahepatic volume (V_e, in liters) in the early phase after injection, B(t) values are higher than the values calculated from the regression line obtained from Equation 5. The ratios of BD(t) to the amount of extrahepatic ^{99m}Tc-GSA, expressed as LD(t) subtracted from injected dose, were calculated and represented by $f_d(t)$ (no unit), i.e., the ratio of V_e to the actual distribution volume:

$$f_d(t) = \frac{BD(t)}{\text{injected dose} - LD(t)}. \quad \text{Eq. 8}$$

During the first 0.5 min after t_0, $f_d(t)$ was calculated in respective five examinations by using 3 mg and 9 mg of ^{99m}Tc-GSA, their mean values at each point were estimated, and they were subsequently approximated to a cubic function of time (Eq. 33).

Kinetic Model

The kinetic model of ^{99m}Tc-GSA is composed of five ^{99m}Tc-GSA compartments and two unbound receptor compartments: C1, extrahepatic plasma; C2, hepatic plasma; C3, ligand–receptor complex on the cell surface; C4, ligand–receptor complex in the cytoplasm; C5, metabolized ligand in the cytoplasm; C6, unbound receptor on the cell surface; and C7, unbound receptor in the cytoplasm (Fig. 1).

The net transport from C1 to C2 is described thus:

$$T_{1\text{-}2} = Q\left(\frac{D_1}{V_e} f_d(t) - \frac{D_2}{V_h}\right). \quad \text{Eq. 9}$$

Assuming that the ligand in the hepatic plasma and receptors on the cell surface attains equilibrium instantaneously, the following equation was obtained:

$$K_d = \frac{D_2 R_s}{V_h D_3}. \quad \text{Eq. 10}$$

The process of the internalization of ligand–receptor complex was described by using rate constants for internalization and exocytosis:

$$T_{3\text{-}4} = k_{in} D_3 - k_{out} D_4. \quad \text{Eq. 11}$$

Transport from C4 to C5 corresponds to dissociation of the ligand–receptor complex in the cytoplasm, which corresponds to the transport of the receptor from C4 to C7:

$$T_{4\text{-}5} = k_r D_4 . \quad \text{Eq. 12}$$

Assuming that equilibrium between receptors on the cell surface and intracellular receptor pool is attained instantaneously:

$$r_{s\text{-}i} = \frac{R_s + D_3}{R_s + R_i + D_3} = \frac{R_s + D_3}{R_{total} - D_4} . \quad \text{Eq. 13}$$

Therefore, the model was described as the following state equations:

$$\frac{dD_1}{dt} = -T_{1\text{-}2}, \quad \text{Eq. 14}$$

$$\frac{d(D_2 + D_3)}{dt} = \frac{dD_2}{dt} + \frac{dD_3}{dt} = T_{1\text{-}2} - T_{3\text{-}4}, \quad \text{Eq. 15}$$

$$\frac{dD_4}{dt} = T_{3\text{-}4} - T_{4\text{-}5} \quad \text{Eq. 16}$$

and

$$\frac{dD_5}{dt} = T_{4\text{-}5} - k_e D_5. \quad \text{Eq. 17}$$

From Equation 10:

$$D_2 R_s = K_d V_h D_3. \quad \text{Eq. 18}$$

Differentiating this equation in time, Equation 18 becomes:

$$D_2 \frac{dR_s}{dt} + R_s \frac{dD_2}{dt} = K_d V_h \frac{dD_3}{dt} . \quad \text{Eq. 19}$$

From Equation 13:

$$R_s = r_{s\text{-}i}(R_{total} - D_4) - D_3 . \quad \text{Eq. 20}$$

Differentiating this equation in time:

$$\frac{dR_s}{dt} = -r_{s\text{-}i}\frac{dD_4}{dt} - \frac{dD_3}{dt} . \quad \text{Eq. 21}$$

From Equations 15, 19, 20 and 21, dD_2/dt and dD_3/dt were calculated thus:

$$\frac{dD_2}{dt} = \frac{r_{s\text{-}i}D_2(T_{3\text{-}4} - T_{4\text{-}5}) + (K_d V_h + D_2)(T_{1\text{-}2} - T_{3\text{-}4})}{K_d V_h + D_2 + r_{s\text{-}i}(R_{total} - D_4) - D_3} \quad \text{Eq. 22}$$

and

$$\frac{dD_3}{dt} = \frac{-r_{s\text{-}i}D_2(T_{3\text{-}4} - T_{4\text{-}5}) + \{r_{s\text{-}i}(R_{total} - D_4) - D_3\}(T_{1\text{-}2} - T_{3\text{-}4})}{K_d V_h + D_2 + r_{s\text{-}i}(R_{total} - D_4) - D_3} . \quad \text{Eq. 23}$$

The initial conditions were:

$$D_1(0) + \text{injected dose of } {}^{99m}\text{Tc-GSA} \quad \text{Eq. 24}$$

and

$$D_2(0) = D_3(0) = D_4(0) = D_5(0) = 0. \quad \text{Eq. 25}$$

These simultaneous nonlinear differential equations (Eqs. 14, 16, 17, 22 and 23) were solved by the Runge–Kutta–Gill method (*19*).

The amount of ^{99m}Tc-GSA accumulated in the liver was expressed as $D_2(t) + D_3(t) + D_4(t) + D_5(t)$.

Hence, the simulated counting rate in the liver ROI (f(t), in kct/sec) is:

$$f(t) = \frac{L_{total} \times [D_2(t) + D_3(t) + D_4(t) + D_5(t)]}{\text{injected dose}} . \quad \text{Eq. 26}$$

Parameter Estimation

There were 10 parameters in these equations: Q, V_e, V_h, K_d, k_{in}, k_{out}, k_r, k_e, $r_{s\text{-}i}$ and R_{total}. K_d, k_{in}, k_{out}, k_r, k_e and $r_{s\text{-}i}$ were assumed to be the same for all subjects, whereas Q, V_e, V_h and R_{total} were assumed to vary according to the subject. Because the excretion of ^{99m}Tc-GSA into the bile during the first 30 min after injection can be considered negligible, k_e was set at 0.0 min^{-1}. Total plasma volume (TPV, in liters), i.e., $V_e + V_h$, was estimated from the height, body weight and hematocrit (Hct) of each subject (*20*):

$$TPV = [0.3669\ \text{height}^3\ (\text{m}) + 0.03219\ \text{weight (kg)} + 0.6041](1 - \text{Hct}) \quad \text{Eq. 27}$$

in males and

$$TPV = [0.3561\ \text{height}^3\ (\text{m}) + 0.03308\ \text{weight (kg)} + 0.1833](1 - \text{Hct}) \quad \text{Eq. 28}$$

in females.

Variable parameters for each subject were defined as Q_1–Q_5, V_{h1}–V_{h5} and R_{total1}–R_{total5}, and the data from ten ^{99m}Tc-GSA examinations in five healthy volunteers were analyzed simultaneously by the modified Marquardt method, which is a nonlinear least-squares algorithm (*19*).

The $L_{correct}(t)$ values from 0.5 to 30 min after t_0 were used as input data. The weighted sum of squares (SS_w) equaled:

$$SS_w = \sum_{i=1}^{5}\sum_{j=1}^{2}\sum_{k=1}^{n}\frac{[L_{correct}(t_k) - f(t_k)]^2}{\sigma_k^2} , \quad \text{Eq. 29}$$

where n is the number of data points in each examination, j is the series of different dose examinations of each subject and i is the subject's number.

The initial values of the parameters at the start of calculation were as follows: K_d = 0.001, 0.01, 0.05, 0.1 and 0.5 μM, $r_{s\text{-}i}$ = 0.01, 0.05, 0.1 and 0.5, k_{in} = 0.2 min^{-1}, k_n = 0.02 min^{-1}, k_r = 0.03 min^{-1}, Q_1–Q_5 = 1.0 liter/min and R_{total1}–R_{total5} = 0.5 μmol. V_{h1}–V_{h5} were roughly estimated by using Equation 31. The amount of the ligand in the blood was assumed to be expressed by one exponential curve (Eq. 30) within 2 min, and the y-intercept (A, in kct/sec) was estimated by regression analysis from t = 0.5 to t = 2.0 min:

$$L_{total} - L_{correct}(t) = Ae^{-\alpha t}. \quad \text{Eq. 30}$$

At t = 0, the counting rate in hepatic plasma equals $L_{total} - A$. V_h was then calculated from the following equation:

$$V_h = TPV\frac{(L_{total} - A)}{L_{total}} . \quad \text{Eq. 31}$$

Curve fitting was performed to minimize the residual sum of squares (SS_w) by using combinations of initial values of K_d and $r_{s\text{-}i}$. Termination was made when the fractional change in SS_w was less than 1.0×10^{-5}. The systematic error was measured as the reduced chi-square. The variance–covariance matrix was calculated by inverting the design matrix after multiplication by its transpose (*21*). The observational sensitivities that comprise the design matrix were calculated by numerical differentiation by using a

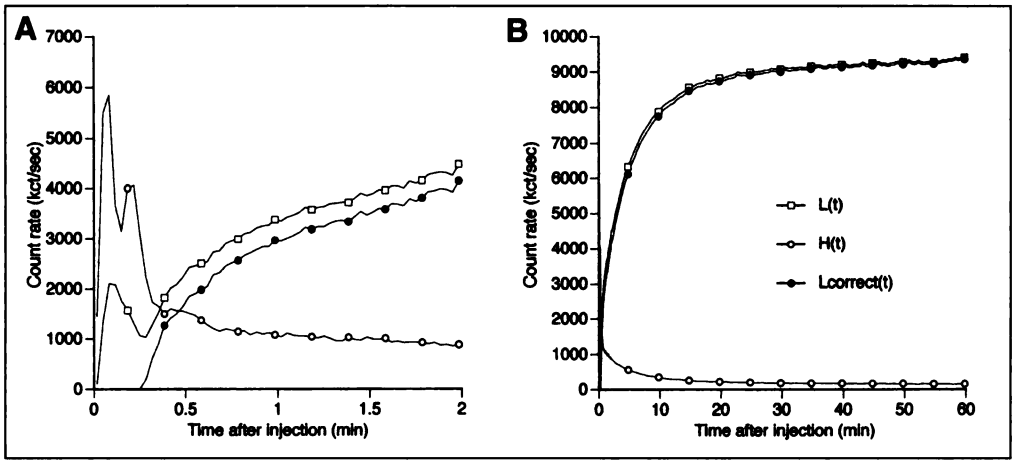

FIGURE 2. Time–activity curves for the heart [H(t)] and liver [L(t) and $L_{correct}(t)$] after a 3-mg dose of ^{99m}Tc-GSA in subject 1. (Not all data points were given symbols.) (A) Time–activity curves within 2 min after injection. L(t) reached its first peak before 15 sec and then increased. (B) Time–activity curves within 60 min after injection. Within 10 min, L(t) increased rapidly up to 84% of the value at 60 min and then increased slowly.

second-order central difference method. The s.e. of each parameter (s.e.p) was estimated as the square root of each diagonal element of the variance–covariance matrix after multiplication by the reduced-chi square for correcting systematic error.

The hepatic plasma flow (Q), receptor amount (R_{total}) and hepatic plasma volume (V_h) of each patient and the healthy volunteers were estimated by using this kinetic model, in which K_d, k_{in}, k_n, k_r and $r_{s\text{-}i}$ were fixed to their best-fit values. In the study of the patients with liver diseases, to estimate errors of parameters caused by the estimated error of L_{total}, the parameters were reestimated after replacing L_{total} with $L_{total} + \Delta L_{total}$. The difference between the original and reestimated parameters (Δp) indicates the error caused by ΔL_{total}. The total error of a parameter was defined as follows:

$$\text{Total error} = (\text{s.e.}_p^2 + \Delta p^2)^{1/2}. \qquad \text{Eq. 32}$$

Data analysis was performed by personal computer using an original program developed by Think C (Symantec Corp., Cupertino, CA).

Model Predictions

After determination of the fixed parameters, the percentage of the injected dose (%ID) in each compartment was calculated by simulation after setting the variable parameters equal to the mean values of healthy volunteers. The effect of the amount of the receptor and hepatic blood flow on the liver uptake curve was evaluated by producing a simulation curve.

Statistical Analysis

Results are expressed as means ± 1 s.d. Student's t-test was used to evaluate the statistical significance of differences between each group, with $p = 0.05$ as the minimum level of significance.

RESULTS

Healthy Volunteers

Dynamic Images and Time–Activity Curve in the Early Phase after Injection. The mean value of t_0 was 13.80 ± 2.04 sec (range 11–17 sec). In all examinations, L(t) reached its first peak before t_0 and increased thereafter (Fig. 2). The ratio of the total counts of L(t) to that of H(t) before t_0 was 0.429 ± 0.19 (range 0.277–0.959).

Validation of the Corrected Heart Time–Activity Curve. At all points measured, H(t)/H(3) and Lu(t)/Lu(3) were greater than BS(t)/BS(3), especially after 15 min, whereas B(t)/B(3) was almost always equal to BS(t)/BS(3) (Fig. 3A) in all examinations in healthy volunteers. Although B(t)/B(3) corresponded to BS(t)/BS(3), with a regression line of $y = 0.013 + 0.953x$ ($R^2 = 0.983$), in the scatter diagram of B(t)/B(3) and H(t)/H(3) against BS(t)/BS(3) of all examinations, H(t)/H(3) did not correspond to BS(t)/BS(3), with a regression line of $y = 0.102 + 0.883x$ ($R^2 = 0.975$) (Fig. 3B). The mean absolute errors of B(t)/B(3) and H(t)/H(3) were 3.4% and 6.9%, respectively. Therefore, the estimated error of B(t) was defined as $0.034 \times B(3)$ (in kct/sec).

Estimation of Absolute Amount of Technetium-99m-GSA in the Liver and Extrahepatic Blood. During the 2–30 min after injection, there was a linear relationship between B(t) and $L_{correct}(t)$ in all examinations in healthy volunteers, but during the first 2 min, B(t) was greater than the corresponding value on the regression line obtained from Equation 5 because of nonuniform distribution of the ligand. After 30 min, $L_{correct}(t)$ was smaller than the corresponding value on the regression line in five examinations, presumably because of excretion of the

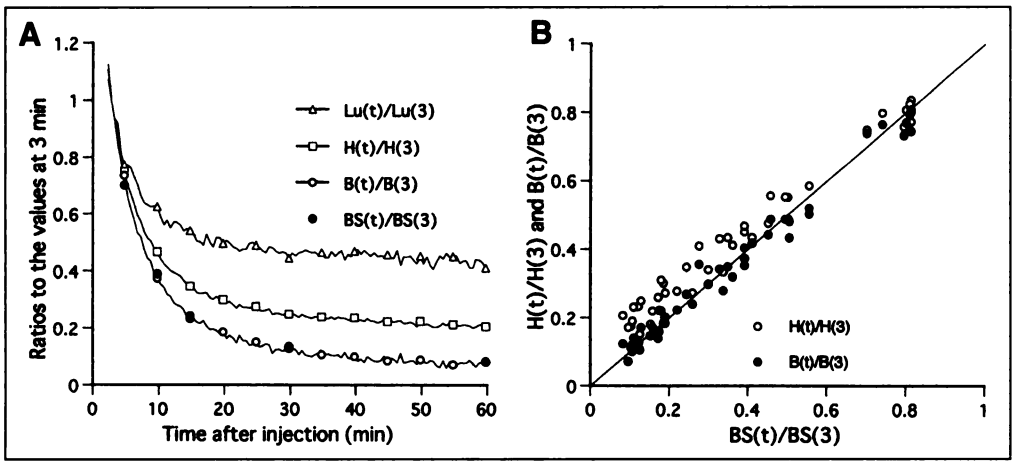

FIGURE 3. (A) Changes in the ratios of the radioactivity of the heart, lung, estimated blood and blood samples to their respective values at 3 min after a 3-mg dose of ^{99m}Tc-GSA (Subject 1). (B) Scatter diagrams of B(t)/B(3) and H(t)/H(3) against BS(t)/BS(3) from all examinations in the five healthy volunteers.

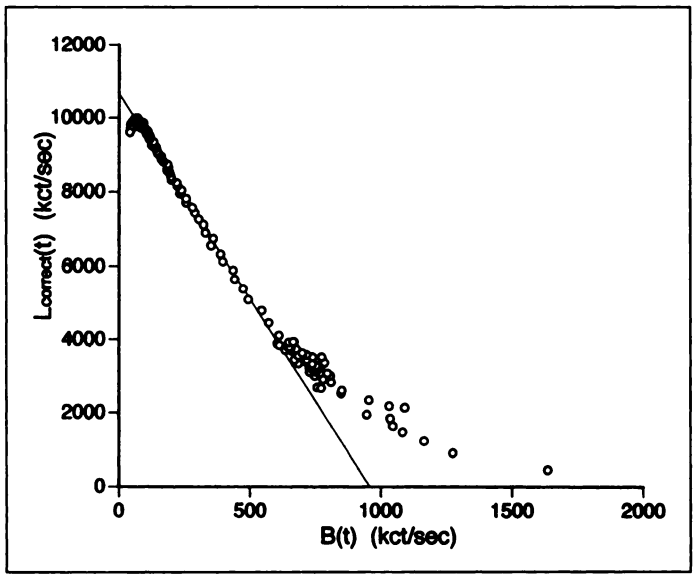

FIGURE 4. Scatter diagram of corrected liver radioactivity [$L_{correct}(t)$] against estimated blood radioactivity [B(t)] after the 9-mg dose of ^{99m}Tc-GSA (Subject 1).

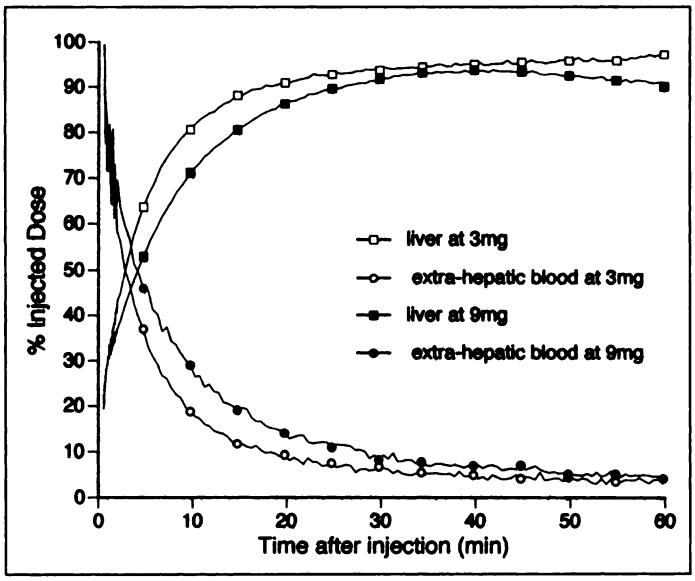

FIGURE 5. Time course of the percentage of the injected dose (%ID) in the liver and extrahepatic blood (Subject 1). Two studies (3 mg and 9 mg) are shown. Not all data points were given symbols.

metabolized ligand to the bile, but was almost always on the regression line in the other five examinations (Fig. 4). The mean of the coefficients of determination of 10 examinations was 0.996. In all subjects, %ID in the liver after the 9-mg dose was smaller than that after the 3-mg dose, whereas the %ID in the blood after the 9-mg dose was larger than that after the 3-mg dose (Fig. 5).

The mean value of $f_d(t)$ of 10 examinations decreased from 2.2 to 1.1 during the first 0.5 min. The regression curve of cubic function of time was obtained by the least-squares method for 0.5 min, in which $f_d(0.5)$ and $df_d(0.5)/dt$ were set at 1.0 and 0.0, respectively:

$$f_d(t) = 4.00(t - 0.5)^3 + 1.788(t - 0.5)^2 + 1.0 \quad \text{for } 0 < t < 0.5,$$

$$f_d(t) = 1.0 \quad \text{for } t \geq 0.5 \qquad \text{Eq. 33}$$

Fixed Parameters. The fitted parameters are shown in Table 2. K_d, k_{in}, k_n and k_r converged on almost the same values by curve fitting using the respective combination of initial values, whereas r_{s-i} varied from 0.0021 to 0.1161. The minimum sum of squares was 24743.7. The best-fit parameters of each subject are shown in Table 3. The mean values for hepatic plasma flow, receptor amount and hepatic plasma volume were 0.916 ± 0.326 liter/min, 0.635 ± 0.079 μmol and 0.314 ± 0.154 liter, respectively. Figure 6 shows the results of curve fitting of liver accumulation in Subject 3.

Model Prediction. Figure 7 shows the %ID of each compartment calculated by simulation using the mean values of the parameters in healthy volunteers (Q = 0.92 liter/min, R_{total} = 0.64 μmol and V_h = 0.31 liter). The ligand–receptor complex on the cell surface increased to 20% of the injected dose at 3 min after injection and then decreased to 4% at 30 min. The internalized ligand–receptor complex increased within 14 min after injection and then decreased slowly. The metabolized ligand increased linearly and reached a value of 42% of the injected dose at 30 min after injection. The liver uptake curve was clearly influenced by the receptor amount (Fig. 8); the %ID at each point in time rose as the receptor amount increased from 0.1 to 0.6 μmol. Although the %ID was, to some extent, influenced by hepatic plasma flow in the normal receptor amount model, there was little difference according to changes in hepatic plasma flow in the reduced receptor amount model (Fig. 9).

Patients with Liver Diseases

Table 4 shows the results of analysis in patients with liver diseases. The R_{total} values were 0.52 ± 0.1 μmol in the N group, 0.34 ± 0.08 μmol in the CH group and 0.16 ± 0.09 μmol in the LC group, and the differences between the N and LC groups ($p < 0.001$), between the N and CH groups ($p < 0.01$) and between the CH and LC groups ($p < 0.005$), were statistically significant. Whereas in the Q values (1.0 ± 0.14 liter/min in the N group, 1.01 ± 0.33 liter/min in the CH group and 0.92 ± 0.50 liter/min in the LC group) or the V_h values

TABLE 2
Parameter Estimation

Parameter	Mean	Minimum	Maximum	Best fit
K_d (μM)	0.0294	0.0267	0.0388	0.0323 ± 0.0019*
K_{in} (min^{-1})	0.5767	0.5517	0.6605	0.6036 ± 0.0566
k_{out} (min^{-1})	0.0490	0.0448	0.0519	0.0463 ± 0.0025
k_r (min^{-1})	0.0294	0.0285	0.0312	0.0286 ± 0.0025
r_{s-i}	0.0309	0.0021	0.1161	0.0610 ± 0.0191
SS_w†	25196.0	24743.7	25776.2	24743.7

*Estimated value ± s.e.
†Degrees of freedom = 940.

TABLE 3
Fitted Parameters of Each Subject

Subject	Q(liters/min)	R_{total}(μmol)	V_h(liters)	SS_w	df*
1	1.494 ± 0.044†	0.710 ± 0.004	0.193 ± 0.021	4156.7	191
2	0.803 ± 0.040	0.636 ± 0.004	0.127 ± 0.019	6719.5	193
3	0.700 ± 0.047	0.511 ± 0.005	0.343 ± 0.023	3300.8	191
4	0.788 ± 0.049	0.622 ± 0.005	0.397 ± 0.024	5202.8	193
5	0.794 ± 0.037	0.695 ± 0.004	0.508 ± 0.020	5363.9	192
Mean	0.916 ± 0.043	0.635 ± 0.004	0.314 ± 0.021	4948.7	
s.d.	0.326 0.005	0.079 0.000	0.154 0.002	1295.7	

*Degrees of freedom.
†Estimated value ± s.e.

(0.29 ± 0.24 liter in the N group, 0.36 ± 0.11 liter in the CH group and 0.19 ± 0.09 liter in the LC group), the differences between any two of the three groups were not statistically significant. The standard errors of Q values in the LC group (1.69 ± 1.83 liter/min) were larger than in the N group (0.162 ± 0.105 liter/min) and in the CH group (0.36 ± 0.18 liter/min).

DISCUSSION

Technetium-99m-GSA is a radiopharmaceutical of ASGP developed for clinical hepatic imaging to evaluate hepatic function (*12*). By using radiolabeled ASGP, hepatic blood flow and ASGP-R were quantitatively assessed by Vera et al. (*15*) in 1984 and by Ha-Kawa et al. (*17*) in 1991, but neither model included receptor recycling and receptor endocytosis, which had been already investigated in detail in in vitro and in vivo experiments (*3–10*). Because the ligand–receptor complex internalized within a few minutes (*22*) and the number of the surface receptors were maintained constant by the receptor recycling (*8*), these mechanisms should be considered in pharmacokinetic analysis of ^{99m}Tc-GSA.

Before analyzing ^{99m}Tc-GSA kinetics by using a multicompartment model, it is necessary to estimate the absolute amount of ^{99m}Tc-GSA in the liver and in extrahepatic blood from the radioactivity of ROIs. To estimate these amounts, the method of Vera et al. (*15*) requires blood sampling, and the method of Ha-Kawa et al. (*17*) necessitates standard counts or whole-body counts. In contrast, our method consists of a three-step procedure, which requires only dynamic image data. First, the liver time–activity curve is corrected by using dynamic images in the early phase after injection. Even after bolus injection, it takes a few seconds for the ligand to reach the liver. L(t) yielded the first peak before t_0, and this may be attributable to extrahepatic radioactivity. Therefore, L(t) was corrected by subtracting H(t), according to the ratio of total counts of L(t) to that of H(t) before t_0. Second, to eliminate the influence of radioactivity in the liver, H(t) was corrected by subtracting Lu(t) according to the modified Ha-Kawa method (*23*). Finally, we estimated the amount of ^{99m}Tc-GSA in the liver based on the linear correlation of B(t) and $L_{correct}(t)$. Assuming that the ligand in the liver or in the heart is distributed uniformly, the shapes of both time–activity curves are not influenced by body or liver shape. In fact, there was an exact linear relationship between B(t) and $L_{correct}(t)$ from 2 to 30 min after injection. During the first 2 min after injection, however, B(t) was larger than the corresponding values on the regression line, indicating nonuniform distribution of ^{99m}Tc-GSA in the blood. We, therefore, calculated the coefficient curve of the ratio of V_e to the actual distribution volume as a cubic function of time and corrected the concentration in the blood for the kinetic analysis.

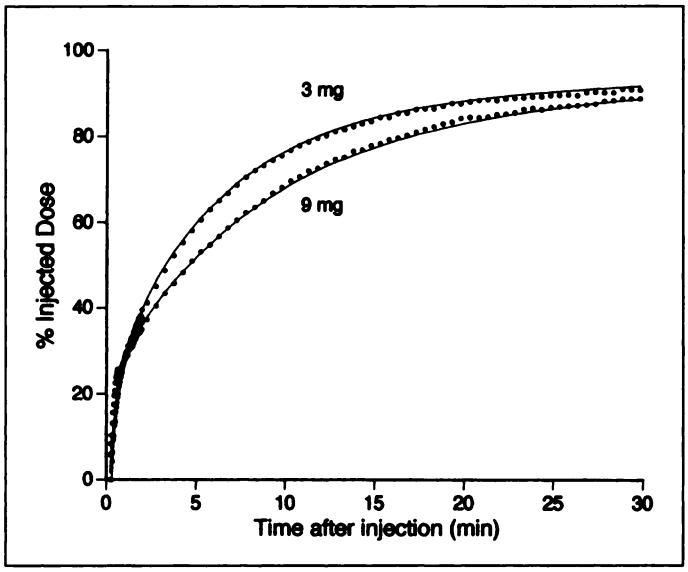

FIGURE 6. Result of curve fitting of liver accumulation after 3 mg and 9 mg doses (Subject 3). Closed circles represent the %ID in the liver of at points measured, and the solid lines represent the approximate curves obtained by curve fitting.

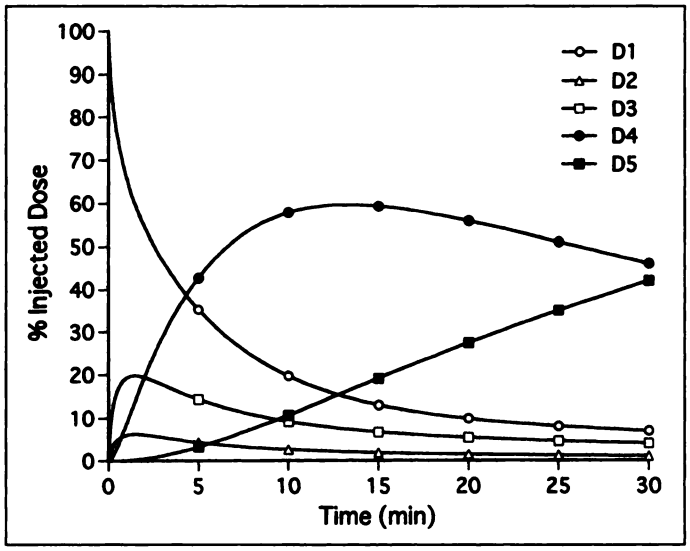

FIGURE 7. The %ID calculated by simulation using the mean values of parameters of healthy volunteers (Q = 0.92 liter/min, R_{total} = 0.64 μmol, V_h = 0.31 liter and V_e = 1.8 liter). The amount of ligand–receptor complex on the cell surface (D3) increased rapidly up to 20% within 2 min and then decreased due to internalization. The internalized ligand–receptor complex (D4) increased within 14 min and then decreased slowly. Intracellular metabolized ligand (D5) increased linearly and reached 42%.

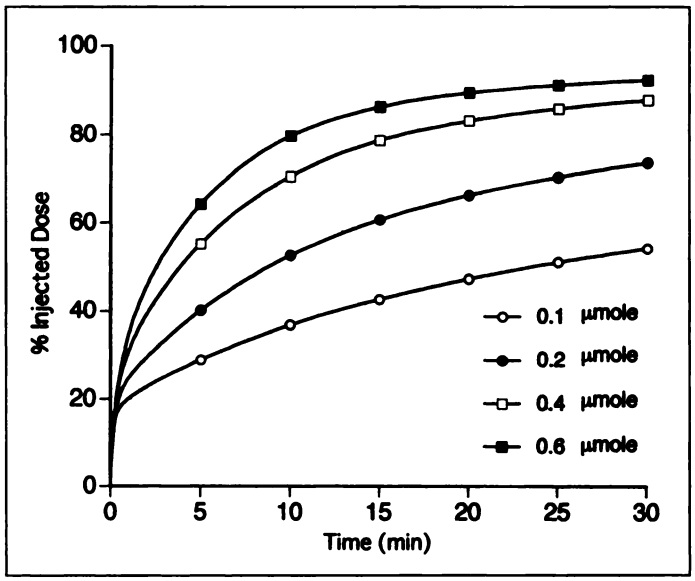

FIGURE 8. The time course of %ID in the liver at various receptor amounts calculated by simulations. The other parameters were fixed to the mean values of parameters of healthy volunteers (Q = 0.9 liter/min, V_h = 0.3 liter and V_e = 1.8 liter). The liver uptake curve was significantly influenced by the receptor amount; the %ID of the liver accumulation at each time point rose as the receptor amount was increased from 0.1 to 0.6 μmol.

Our kinetic model represents the cellular transport of ASGP and ASGP-R by introducing several assumptions. At first, because the process of binding of the ligand to the surface receptor was thought to be faster than the internalization process (*10*), the rapid equilibrium between the ligand and the surface receptors was assumed. Second, the first-order kinetics of endocytosis (*6,8,10*) and exocytosis (*24,25*) of the ligand–receptor complex were assumed in the internalization process. The receptor recycling mechanism was represented by assuming a rapid equilibrium between the surface receptor and intracellular receptor pool.

There are many parameters in our compartment model, and these various parameters correlated with each other. We therefore prepared fixed and changeable parameters, thereby enabling the precise estimation of the amount of receptor and hepatic plasma flow. The parameters for chemical reactions in hepatocytes were assumed to be fixed based on the intact hepatocyte theory (*26,27*). We determined these fixed parameters by analyzing data from five healthy volunteers at different doses simultaneously by using the nonlinear least-squares method. Although we performed curve fittings with many combinations of initial values, the fixed parameters, excepting r_{s-i}, converged at almost the same values from all combinations of initial values, indicating that the fixed parameters had been successfully estimated. Although the values of the fixed parameters had been reported in various experiments in vitro and in vivo, these values varied because of different experimental conditions. The K_d values reported varied from 5.0×10^{-10} *M* to 3.4×10^{-8} *M*, and our results yielded a value of 3.07×10^{-8} *M*, which was similar to that reported by Steer and Ashwell (*28*). The rate constants for endocytosis and exocytosis were estimated to be 0.6 min^{-1} and 0.04 min^{-1}, respectively. The exocytotic pathway has been reported by many investigators, and our results supported the kinetics of the "rapid transit pool" with $t_{1/2}$ = 28 min, reported by Simmons and Schwartz (*24*). The ratio of the surface receptors to the receptor pool were estimated to be 6.1%, which ranged from 5% (*4*) to 35% (*28*) in different reports. The mean value of the total amount of receptor of healthy volunteers was estimated to be 0.6 μmol. Although this five-fold is greater than the value estimated by the model of Vera et al. (*16*), it may be reasonable provided that only the surface receptor fraction was estimated in this method. In the simulation of each compartment by using the mean values for the changeable parameters of healthy volunteers, the ligand–receptor complex on the cell surface increased to only 20% of the injected dose, and it was immediately internalized. The internalized ligand–receptor complex increased up to 60% and then decreased gradually. The time course of the distribution of each compartment was compatible with other in vitro results (*8*).

We also assessed the effect of the receptor amount and hepatic blood flow on the liver uptake curve and found that it was significantly influenced by the receptor amount. It was also influenced by hepatic blood flow to some extent when the liver uptake curve was simulated by setting the mean receptor amount equal to that in healthy volunteers, but it was less influenced in cases with decreased receptor amount. The analysis in patients with liver diseases yielded statistically significant differences between the three groups in the R_{total} values, but not in the Q or V_h values. The s.e. values of the Q values in the LC group were very large, but those of the R_{total} values were very small. These results indicate that the receptor amount can be accurately estimated in both normal and cirrhotic livers, whereas hepatic blood flow cannot be estimated pre-

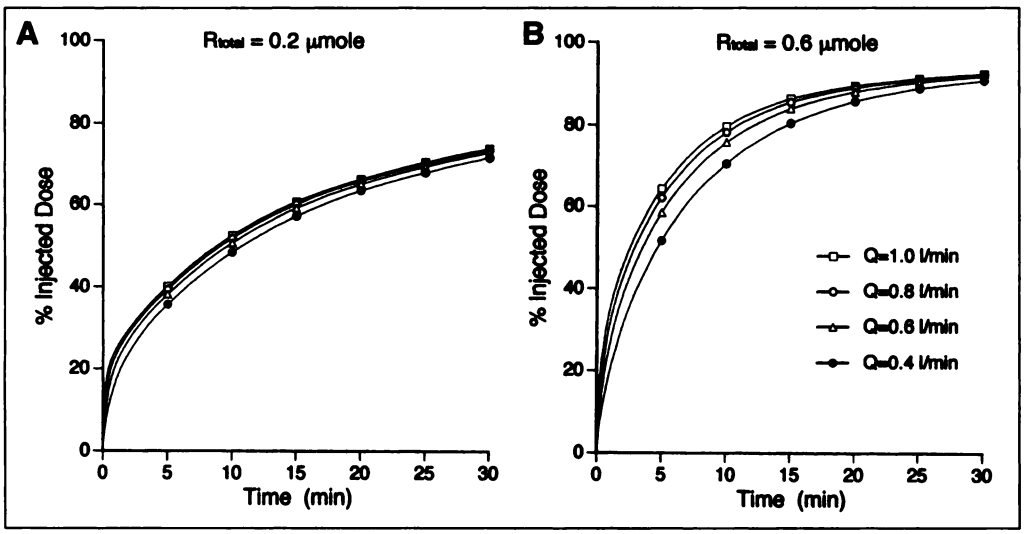

FIGURE 9. The time course of %ID of liver accumulation at various hepatic plasma flows at two receptor amounts. At the decreased receptor amount (A), the hepatic plasma flow influenced the curves less than at the normal receptor amount (B).

TABLE 4
Parameter Estimation in Patients with Liver Diseases

Patient no.	Age/sex	Liver disease	R_{total} (μmol)	Q (liters/min)	V_h (liters)	SS_w	df	Reduced Chi-square	CV (%)
N group (n = 5)									
1	63/M	Liver metastasis	0.429 ± 0.021*	1.131 ± 0.171	0.122 ± 0.040	599.5	93	6.45	0.629
2	60/M	Liver metastasis	0.676 ± 0.036	1.129 ± 0.102	0.151 ± 0.078	271.0	91	2.98	0.4
3	47/M	Liver metastasis	0.471 ± 0.041	0.863 ± 0.335	0.696 ± 0.188	2709.0	95	28.52	1.34
4	60/F	Liver metastasis	0.434 ± 0.010	0.835 ± 0.065	0.154 ± 0.031	484.5	91	5.32	0.552
5	58/M	Liver metastasis	0.605 ± 0.041	1.056 ± 0.134	0.322 ± 0.117	521.5	89	5.86	0.651
CH group (n = 6)									
6	76/M	CH	0.295 ± 0.015	1.645 ± 0.512	0.228 ± 0.048	359.5	92	3.91	0.512
7	55/M	CH	0.304 ± 0.016	0.743 ± 0.211	0.371 ± 0.080	734.4	90	8.16	0.847
8	50/M	CH	0.469 ± 0.023	1.031 ± 0.068	0.245 ± 0.041	211.5	88	2.40	0.374
9	78/M	CH	0.230 ± 0.012	0.742 ± 0.435	0.512 ± 0.142	3320.0	91	36.48	1.732
10	66/M	CH HCC	0.327 ± 0.020	0.989 ± 0.424	0.434 ± 0.111	1685.1	94	17.93	1.175
11	49/M	CH HCC	0.393 ± 0.032	0.925 ± 0.509	0.390 ± 0.176	1523.2	91	16.74	1.287
LC group (n = 8)									
12	52/F	LC	0.290 ± 0.014	0.667 ± 0.107	0.247 ± 0.043	480.3	86	5.58	0.591
13	81/M	LC HCC	0.151 ± 0.009	1.379 ± 0.673	0.157 ± 0.020	191.4	93	2.06	0.333
14	60/F	LC	0.206 ± 0.012	0.586 ± 0.329	0.292 ± 0.088	1249.6	89	14.04	1.107
15	72/M	LC HCC	0.247 ± 0.009	0.374 ± 0.051	0.075 ± 0.047	285.1	91	3.13	0.716
16	43/M	LC	0.088 ± 0.010	1.179 ± 2.490	0.235 ± 0.058	142.1	91	1.56	0.533
17	68/M	LC	0.107 ± 0.011	1.356 ± 4.144	0.220 ± 0.119	596.7	89	6.70	1.129
18	74/M	LC	0.112 ± 0.010	1.514 ± 4.590	0.225 ± 0.109	477.9	89	5.37	1.048
19	60/F	LC	0.043 ± 0.007	0.270 ± 1.112	0.056 ± 0.047	470.6	83	5.67	1.683
N group									
Mean			0.523 ± 0.030	1.003 ± 0.162	0.289 ± 0.091	917.1		9.82	0.714
s.d.			0.111 0.014	0.144 0.105	0.241 0.064	1009.1		10.53	0.363
CH group									
Mean			0.336 ± 0.020	1.013 ± 0.360	0.363 ± 0.100	1305.6		14.27	0.988
s.d.			0.083 0.007	0.333 0.180	0.110 0.053	1154.8		12.64	0.510
LC group									
Mean			0.155 ± 0.010	0.916 ± 1.687	0.188 ± 0.066	486.7		5.51	0.892
s.d.			0.085 0.002	0.495 1.832	0.085 0.035	346.7		3.92	0.433

*Estimated value ± s.e.

M = male; F = female; df = degrees of freedom; CV = coefficient of variation for total residual error; CH = chronic hepatitis; LC = liver cirrhosis; HCC = hepatocellular carcinoma.

cisely in cirrhotic patients, which was also observed with the method of Vera et al. (*29*).

CONCLUSION

In this study, we presented one kinetic model of cellular transport of ASGP and ASGP-R. However, the validity of the fixed parameter values and the estimated receptor amount were not confirmed. Therefore, further investigation is necessary.

Compared to the current methods, our kinetic model, which incorporates receptor-mediated endocytosis and receptor recycling more accurately reflects the biochemistry of ASGP-R. This method, by using this kinetic model, permits the quantitative measurement of the receptor amount and hepatic blood flow by analyzing dynamic images of ^{99m}Tc-GSA without blood samples. Therefore, liver functional reserve in terms of the receptor amount, exclusive of the effect of hepatic blood flow, can be evaluated by using this method.

ACKNOWLEDGMENTS

This work was supported by a Grant-in-Aid for scientific research from the Ministry of Health and Welfare of Japan (Grant 08407036). We thank Nihon Medi-Physics Co., Ltd. (Nishinomiya, Japan) for supplying ^{99m}Tc-GSA.

REFERENCES

1. Morell AG, Ivrine RA, Sternlieb I, Scheunberg IH, Ashwell G. Physical and chemical studies on celuroplasmin. V. Metabolic studies on sialic acid free cerloplasmin in vivo. *J Biol Chem* 1968;243:155–159.
2. Pricer WE, Ashwell G. The binding of desialylated glycoproteins by plasma membranes of liver. *J Biol Chem* 1971;246:4825–4833.
3. Weigel PH. Characterization of the asialoglycoprotein receptor on isolated rat hepatocytes. *J Biol Chem* 1980;255:6111–6120.
4. Steer CJ, Ashwell G. Studies on a mammalian hepatic binding protein specific for asialoglycoproteins. *J Biol Chem* 1980;255:3008–3013.
5. Schwartz AL, Fridovich SE, Knoweles BB, Lodish HF. Characterization of the asialoglycoprotein receptor in a continuous hepatoma line. *J Biol Chem* 1981;256: 8878–8881.
6. Schwartz AL, Fridovich SE, Lodish HF. Kinetics of internalization and recycling of the asialoglycoprotein receptor in a hepatoma cell line. *J Biol Chem* 1982;257:4230–4237.
7. Weigel PH, Oka JA. Temperature dependence of endocytosis mediated by the asialoglycoprotein receptor in isolated rat hepatocytes. *J Biol Chem* 1981;256:2615–2617.
8. Bridges K, Harford J, Ashwell G, Klausner RD. Fate of receptor and ligand during endocytosis of asialoglycoproteins by isolated hepatocytes. *Proc Natl Acad Sci USA* 1982;79:350–354.
9. Appel M, Potrat P, Feger J, Mas-Chamberlin C, Durand G. In vivo quantification of removal of asialo-orsomucoid from the circulation in anesthetized streptozotocin-diabetic rats. *Diabetologia* 1986;29:383–387.
10. Weigel PH, Oka JA. Endocytosis and degradation mediated by the asialoglycoprotein receptor in isolated rat hepatocytes. *J Biol Chem* 1982;257:1201–1207.
11. Sawamura T, Nakada H, Hazama H, Shiozaki Y, Sameshima Y, Tashiro Y. Hyperasialoglycoproteinemia in patients with chronic liver diseases and/or liver cell carcinoma. *Gastroenterology* 1984;87:1217–1221.
12. Torizuka K, Ha-Kawa SK, Ikekubo K, et al. Phase I clinical study on ^{99m}Tc-GSA, a

new agent for functional imaging of the liver [Japanese]. *Kaku-igaku* 1991;28:1321–1331.
13. Kudo M, Todo A, Ikekubo K, et al. Functional hepatic imaging with receptor-binding radiopharmaceutical: clinical potential as a measure of functioning hepatocyte mass. *Gastroenterol Jpn* 1991;26:734–741.
14. Koizumi K, Uchiyama G, Arai T, Ainoda T, Yoda Y. A new functional study using ^{99m}Tc-DTPA galactosyl human serum albumin: evaluation of the validity of several functional parameters. *Ann Nuklearmedizin* 1992;6:83–87.
15. Vera DR, Krohn KA, Stadalnik RC, Sceibe PO. Technetium-99m-galactosyl-neoglycoalbumin: in vitro characterization of receptor-mediated binding. *J Nucl Med* 1984;25:779–787.
16. Vera DR, Stadalnik RC, Trudeau WL, Scheibe PO, Krohn KA. Measurement of receptor concentration and forward-binding rate constant via radiopharmacokinetic modeling of technetium-99m-galactosyl-neoglycoalbumin. *J Nucl Med* 1991;32:1169–1176.
17. Ha-Kawa SK, Tanaka Y. A quantitative model of technetium-99m-DTPA galactosyl-HSA for the assessment of hepatic blood flow and hepatic binding receptor. *J Nucl Med* 1991;32:2233–2240.
18. Press WH, Flannery BO, Teukolsky SA, Vetterling WT. Straight-line data with errors in both coordinates. In: Press WH, Flannery BO, Teukolsky SA, Vetterling WT, eds. *Numerical recipes in C: the art of scientific computing*, 2nd ed. Cambridge, UK: Cambridge University Press; 1992:666–670.
19. Yamaoka K, Nakagawa T. A nonlinear least squares program based on different equations, MULTI (RUNGE), for microcomputers. *J Pharmacobiodyn* 1983;6:595–606.
20. Nadler SB, Hidalgo JU, Bloch T. Prediction of blood volume in normal adults. *Surgery* 1962;51:224–232.
21. Press WH, Flannery BO, Teukolsky SA, Vetterling WT. Solution by use of the normal equations. In: Press WH, Flannery BO, Teukolsky SA, Vetterling WT, eds. *Numerical recipes in C: the art of scientific computing*, 2nd ed. Cambridge, UK: Cambridge University Press; 1992:672–675.
22. Hubbard AL, Stukenbrock H. An electron microscope autoradiographic study of the carbohydrate recognition system in rat liver II. Intracellular fate of the ^{125}I-ligands. *J Cell Biol* 1979;83:65–81.
23. Ha-Kawa SK, Kojima M, Suga Y, Kurokawa H, Itagaki Y, Tanaka Y. Dose estimation of ^{99m}Tc-DTPA galactosyl-human serum albumin (^{99m}Tc-GSA) in the blood with nonlinear regression method [Japanese]. *Kaku Igaku* 1991;28:425–427.
24. Simmons CF, Schwartz AL. Cellular pathways of galactose-terminal ligand movement in a cloned human hepatoma cell line. *Mol Pharmacol* 1984;26:509–519.
25. Tolleshaug H, Chindermi PA, Regoeczi E. Diacytosis of human asialotransferrin type 3 by isolated rat hepatocytes. *J Biol Chem* 1981;256:6526–6528.
26. Branch RA, James JA, Read AE. The clearance of antipyrine and indocyanine green in normal subjects and in patients with chronic liver diseases. *Clin Pharmacol Ther* 1976;20:81–89.
27. Kawasaki S, Imamura H, Bandai Y, Sanjo K, Idezuki Y. Direct evidence for the intact hepatocyte theory in patients with liver cirrhosis. *Gastroenterology* 1992;102:1351–1355.
28. Steer CJ, Ashwell G. Receptor-mediated endocytosis. Mechanisms, biologic function and molecular properties. In: Zakim D, Boyer TD, eds. *Hepatology: a textbook of liver disease*, 2nd ed. Philadelphia: W.B. Saunders; 1990:137–181.
29. Vera DR, Stadalnik RC, Metz CE, Pimstone NR. Diagnostic performance of a receptor-binding radiopharmacokinetic model. *J Nucl Med* 1996;37:160–164.

Colonic Transit Scintigraphy Labeled Activated Charcoal Compared with Ion Exchange Pellets

Duane D. Burton, Michael Camilleri, Brian P. Mullan, Lee A. Forstrom and Joseph C. Hung
Gastroenterology Research Unit and Section of Nuclear Medicine, Mayo Clinic and Mayo Foundation, Rochester, Minnesota

Scintigraphic measurement of colonic transit is currently performed by delivering ^{111}In ion exchange resin pellets to the colon in a methacrylate-coated capsule. However, use of this method is constrained by the need for an investigational drug permit. We have demonstrated previously optimal adsorption in vitro of commonly used radioisotopes (e.g., ^{99m}Tc or ^{111}In) to activated charcoal in milieus that mimicked gastric and small intestinal content. The aim of this study was to compare the transit profiles of radioactive activated charcoal and resin pellets delivered to the colon in the same methacrylate-coated capsule. **Methods:** In 10 healthy volunteers, we compared the colonic transit profiles over 32 hr of simultaneously administered resin pellets labeled with ^{111}In and activated charcoal mixed with ^{99m}Tc-diethylenetriaminepentaacetic acid. Transit was summarized as the geometric center (weighted average of counts) in the colon at each scanning period. **Results:** Colonic transit profiles were virtually identical with the two markers, with less than 0.1 geometric center unit differences in the transit profiles over the 32-hr periods. **Conclusion:** Activated charcoal is a suitable alternative to resin pellets when delivered in a methacrylate-coated, delayed-release capsule to the colon for measurement of transit by scintigraphy.

Key Words: colonic transit; charcoal; scintigraphy

J Nucl Med 1997; 38:1807–1810

Measurement of colonic transit is a useful clinical and research technique for evaluating patients with suspected motility disorders of the colon. The radiopaque marker method (*1*) is widely available and is relatively inexpensive and reproducible (*2*), but it requires patients to be available for 4–7 days in order to evaluate the transit profile in the colon. The need to have a test with a faster completion time and more detailed assessment of regional colonic motor function has led us to develop a radioscintigraphic approach (*3*) that has since been simplified (*4*) and used clinically (*5*). It involves radiolabeling ion exchange resin pellets with isotopes such as ^{99m}Tc or ^{111}In and delivering these to the colon in a delayed-release, methacrylate polymer-coated medication capsule that dissolves in the alkaline pH of the terminal ileum. These initial research studies also have led to novel insights into the pathophysiology of the colon in diseases such as irritable bowel syndrome, idiopathic constipation and carcinoid diarrhea (*2,6,7*). Clinical utilization of the test (*5*) required a great deal of administrative support to meet regulatory requirements when using radiolabeled pellets under an investigational new drug application. In a clinical venue, this becomes administratively burdensome because the test only can be done after the patient has signed an informed consent form and reduces considerably the cost efficacy of the method; moreover, reimbursement by third-party payers is complicated because the informed consent is required to use the markers with an investigational new drug.

Our aim was to develop a new marker to be used in measuring colonic transit in human subjects. The characteristics of such a new marker would need to match the ideal properties we have previously noted when using labeled ion exchange pellets (*3–5*). The method would ideally involve "radiolabeling," a substrate that fulfills U.S. Pharmacopeia standards for synthesis; moreover, radiolabeling should be achieved with one of the commonly used radioisotopes, ^{99m}Tc or ^{111}In. The association between radioisotope and substrate must be optimal in the ranges of pH between 2 and 7.5 that are observed in the gastrointestinal tract and in the presence of pancreatic enzymes and conjugated bile acids. Finally, the marker's colonic transit

Received Sep. 16, 1996; revision accepted Jan. 13, 1997.
For correspondence or reprints contact: Michael Camilleri, MD, Mayo Clinic, Gastroenterology Unit, Alfred 2–435, 200 First St. S.W., Rochester, MN 55905.